Journal of Power Sources 195 (2010) 729–735

Contents lists available at ScienceDirect

Journal of Power Sources

journal homepage: www.elsevier.com/locate/jpowsour

Electrocatalytic activity of Pt nanoparticles electrodeposited on amorphous carbon-coated silicon nanocones

Jitendra N. Tiwari [a], Fu-Ming Pan [a,*], Te-Ming Chen [a], Rajanish N. Tiwari [a], Kun-Lin Lin [b]

[a] Department of Materials Science and Engineering, National Chiao Tung University, 1001 Ta Hsueh Road, Hsinchu 30050, Taiwan, ROC
[b] Department of Mechanical Engineering, National Taiwan University of Science and Technology, Taipei 0660, Taiwan, ROC

ARTICLE INFO

Article history:
Received 14 July 2009
Received in revised form 11 August 2009
Accepted 13 August 2009
Available online 20 August 2009

Keywords:
Platinum
CO oxidation
Methanol oxidation
Oxygen reduction reaction

ABSTRACT

This study pulse-electrodeposits Pt nanoparticles on amorphous carbon-coated silicon nanocones (ACNCs) and explores them as the electrocatalyst for methanol oxidation reaction (MOR) and oxygen reduction reaction (ORR) for direct methanol fuel cell applications. The work prepares silicon nanocones on the Si wafer using porous anodic aluminum oxide as the template and then deposits the amorphous carbon layer on the nanocones by microwave plasma chemical vapor deposition. According to Raman scattering and X-ray photoelectron spectroscopies (XPS), the surface of the ACNC support is composed of a nanocrystalline graphitic structure, and rich in oxygen-containing adspecies. The Pt nanoparticles pulse-electrodeposited on the highly ordered ACNC support disperses well with a large electrocatalytic surface area. The Pt/ACNC electrode exhibits excellent electrocatalytic activity and stability toward both MOR and ORR. This study suggests the abundant oxygen-containing surface species and the nanometer size of the Pt catalyst as the two major factors enhancing electrocatalytic performance of Pt/ACNC electrode. The XPS study suggests the occurrence of charge transfer from π-sites of the graphitic structure to the Pt nanoparticle, thereby improving the electrochemical stability of the electrode.

© 2009 Elsevier B.V. All rights reserved.

1. Introduction

Since direct methanol fuel cells (DMFCs) can operate at relatively low temperatures, and are lightweight and power efficient, they are very attractive for mobile power source applications, such as automotive systems and portable electronics. Significant progress has been made over the past decade to enhance the electrochemical performance of DFMCs. However, low methanol oxidation reaction (MOR) activity, poor kinetics of the oxygen reduction reaction (ORR), and high cost of Pt-based electrocatalysts still pose a great challenge for commercialization. Different approaches have attempted to improve electrocatalytic activity to reduce precious Pt catalyst usage and increase electrocatalytic activity for MOR and ORR. To achieve this goal, well-dispersed Pt catalyst nanoparticles are usually deposited on the catalyst support with a large surface area. Because carbon materials can usually be prepared to have a large surface area for Pt loading, they have been widely used as the support for the Pt catalyst, such as nanoporous graphite with Pt nanoparticles [1], carbon nanocoils with Pt–Ru catalyst alloys [2] and carbon-coated anatase TiO_2 composites [3]. Carbon materials generally have a high content of oxygen surface groups, which act as anchoring centers for the Pt precursor and thus improve wetability of the Pt precursor on the carbon support, resulting in better Pt dispersion [4]. The large support surface and highly dispersed nanosized Pt catalyst create a large effective electrocatalytic surface area and, therefore, greatly enhance ORR and MOR activities. Many studies have shown that carbon support significantly enhances MOR and ORR activities and Pt catalyst stability [5–7].

Amorphous carbon (α-C) has a wide range of industrial applications because of many attractive material properties, such as mechanical hardness, chemical inertness, wear resistance and optical transparency. Different hybridizations of C atoms in α-C result in an electronic structure mixed with sp^2 as well as sp^3 bonding, and the short range sp^2 hybridization leads to the formation of π and π* bands in nm-sized carbon clusters [8]. The presence of π-bonding sites on a carbon support can improve Pt–C adhesion strength, alleviating agglomeration and loss of Pt catalyst particles during electrochemical reactions [9–11]. In the study, we prepared α-C coated nanostructured supports for Pt loading, and studied electrocatalytic performance of the nanostructured electrode in MOR and ORR for DMFC applications. The electrocatalyst support is a highly ordered silicon nanocone (SNC) array coated by an ultrathin α-C surface layer, which provides a large surface area for Pt loading. Pt catalyst particles of nanometer scale were deposited on the nanocones by potentiostatic bipolar pulse electrodeposition. Because the α-C coated Si nanocone (ACNC) array is fabricated directly on a low resistivity Si substrate (0.002 μΩ cm), which acted

* Corresponding author. Tel.: +886 3 5131322; fax: +886 3 5724727.
E-mail address: fmpan@faculty.nctu.edu.tw (F.-M. Pan).

0378-7753/$ – see front matter © 2009 Elsevier B.V. All rights reserved.
doi:10.1016/j.jpowsour.2009.08.030

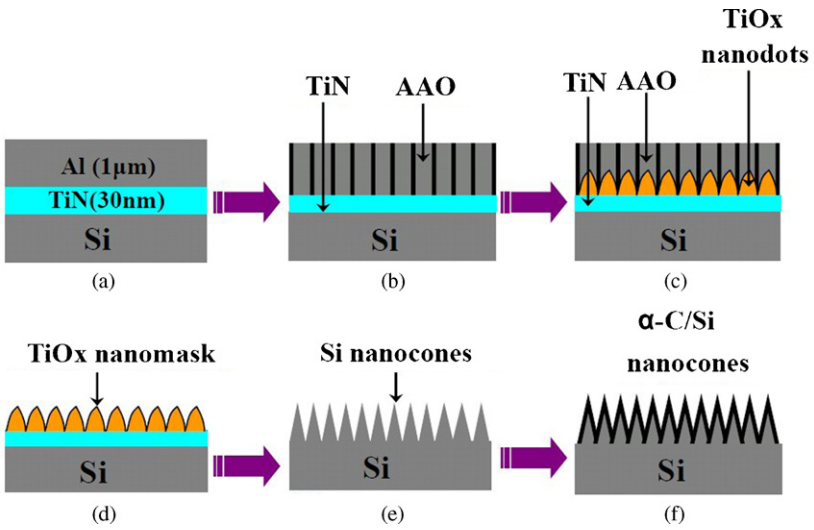

Fig. 1. Fabrication processes of the ordered ACNC array: (A) deposition of TiN and Al thin films on the Si wafer by sputter deposition and thermal evaporation, respectively, (B) formation of the porous AAO template, (C) formation of TiO_x nanodots in the AAO pore channels, (D) removal of AAO by wet etch, (E) RIE of the remaining TiN and silicon substrate, forming Si nanocones, and (F) deposition of α-C on SNCs by MPCVD.

as the current collector, the ACNC support is very suitable for use as the Pt electrocatalytic electrode (thereafter denoted as the Pt/ACNC electrode). In a previous work, we found that Pt nanoparticles pulse-electrodeposited on bare SNCs had a high electrocatalytic activity toward MOR with a good electrochemical stability [12]. The study shows that the Pt/ACNC electrode exhibits a comparable electrocatalytic activity toward MOR with a better electrochemical stability.

2. Experimental

2.1. Fabrication procedure of the ACNC array

The SNC array fabrication procedure has been reported in detail previously [12,13]. Fig. 1 shows schematically the fabrication procedure. A p-type 4-in. Si wafer of low resistivity (0.002 Ω cm) was used as the substrate. A TiN thin film 30 nm thick was first sputter-deposited on the Si surface, followed by thermal evaporation of an aluminum thin film 1 μm thick. The TiN layer was used as the adhesion layer between the Si substrate and the Al thin film, and later used for preparing the nanodot mask for fabricating the SNC array. The as-deposited Al/TiN film stack was then oxidized by electrochemical anodization, performed in a 0.3 M oxalic acid ($H_2C_2O_4$) aqueous solution at 25 °C under a constant polarization voltage of 40 V for 20 min. Anodic oxidation of the Al thin film under the anodization conditions produced hexagonally arranged anodic aluminum oxide (AAO) nanopore channels. As the anodization reaction approached the interface between the Al and TiN thin films, local anodization of the underlying TiN layer occurred, forming the TiO_2 nanodot mask on the TiN layer. The AAO was then removed by the aqueous solution of 6 wt% H_3PO_4 and 1.5 wt% CrO_3 at 70 °C for 40 min. With the remaining TiO_2 nanodots as the mask, the TiN capped Si substrate was etched by inductively coupled-plasma reactive-ion-etch (RIE) for 40 s using a gas mixture of BCl_3 and Cl_2 as the plasma source. The RIE process was performed under the following working conditions: plasma power 400 W, substrate bias power 120 W, working pressure 10 mTorr with a flow rate of 35 sccm for the plasma gas source. Deposition of the α-C on the SNC array was carried out by microwave plasma chemical vapor deposition (MPCVD) with the following deposition conditions: the CH_4:H_2 gas flow rate ratio 20:80 sccm, plasma power 300 W, bias power 200 W, working pressure 1 Torr, and deposition time 25 min.

2.2. Electrodeposition of Pt nanoparticles

Pt nanoparticles were electrodeposited on the ACNC array in the aqueous solution of 1 M K_2PtCl_6/0.5 M HCl at room temperature by potentiostatic pulse plating in a three electrode cell system with a saturated calomel reference electrode (SCE). The highly ordered ACNC array was the working electrode and the counter electrode was a thin Pt wire. The particle size and dispersion of Pt nanoparticles was controlled by tuning the pulse height of the applied potential and the pulse duration. The time durations for the high potential pulse (−0.08 mV) and the low potential pulse (+0.01 mV) were 7 and 1 ms, respectively. The mass loading of the Pt catalyst on the ACNC electrode was determined by measuring the difference in the mass of the ACNC electrode before and after Pt deposition, using a micro-balance (Sartorious, PB-SAH) with a resolution of 0.001 mg. Under the pulse electrodeposition condition, the typical Pt loading on the ACNC support was ∼0.028 mg cm^{-2}.

2.3. Electrochemical measurements

Electrochemical measurements were conducted in the same three-electrode cell at room temperature. All aqueous solutions were prepared using low resistance ∼18 MΩ DI water produced by a Milli-Q water purification system. The Pt/ACNC electrode was rinsed thoroughly with deionized water to remove residual chlorine ions after Pt electrodeposition, and allowed to dry before being used for electrochemical measurements. The CO adsorption on the Pt catalyst was performed by flowing the 10% CO/N_2 gas mixture in the 1 M H_2SO_4 aqueous solution at 100 mV for 35 min. Before the CO-stripping measurement, the solution was purged with N_2 gas for 30 min to remove CO remaining in the solution.

2.4. Physico-chemical characterization

Surface morphology of the samples was examined by scanning electron microscopy (SEM, JEOL JSM-6700F). Transmission electron microscopy (TEM, JEOL JEM-3000F) was used to analyze crystallinity and particle size distribution of Pt nanoparticles. The TEM specimens were prepared by scratching Pt deposited ACNC nanocones off the Si substrate with a pair of dissecting forceps in the presence of a small drop of ethanol, and then put onto a holly-copper grid and dried in air at room temperature. X-ray pho-

toelectron spectroscopy (XPS, Thermo VG 350) was performed with the Mg Kα radiation (1253.6 eV) to study the chemical composition of the Pt/ACNC electrode. Raman spectroscopy (Jobin Yvon LabRam HR system) using the He–Ne laser as the excitation source was used to analyze chemical structure of the α-C layer on the ACNC array.

3. Results and discussion

3.1. Material properties of the Pt–ACNC electrode

The α-C coated SNCs fabricated by the AAO templation method had a highly ordered hexagonal arrangement. Fig. 2(A) and (B) shows SEM images of the ordered ACNC array before and after the electrodeposition of Pt nanoparticles. The well ordered nanocones were ~250 nm in height and had a base diameter of ~100 nm. The ACNCs provided a surface area applicable for Pt loading about five times (the ratio of the cone surface area to the cone base area) that of a flat Si substrate. Pt loading on the nanocone electrode by potentiostatic bipolar pulse electrodeposition is an effective approach to deposit crystalline nanoparticles of well-controlled quality on the cathode. The highly ordered ACNC arrangement allowed a relatively uniform potential distribution over the nanocone array in the electrolyte, crucial for electrodeposition of well-dispersed Pt nanoparticles on the ACNC cathode. Because Pt nanoparticles on the ACNC support were very small and without obvious agglomeration, the SEM image of Fig. 2(B) hardly observed the Pt nanoparticles. Fig. 3(A) shows the bright-field TEM image of the ACNC with the electrodeposited Pt catalyst. The figure clearly shows that Pt nanoparticles were well dispersed on the nanocones. According to the high-resolution TEM image (Fig. 3(B)), most of the deposited Pt nanoparticles had a size smaller than 5 nm. Fig. 3(C) shows the selected area electron diffraction (SAD) pattern. The distinct diffraction spots in the SAD image were due to the crystalline Si nanocone substrate. Two diffraction rings of discernible intensity were indexed as the (1 1 1) and (2 0 0) lattice planes of the Pt face center cubic (FCC) structure. The diffraction rings corresponding to

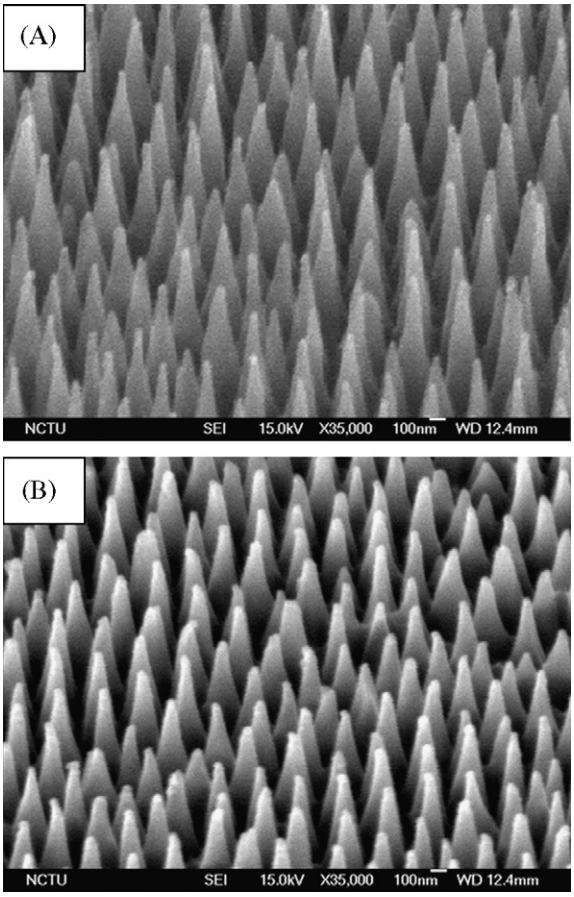

Fig. 2. The side-view SEM images of the α-C coated SNC array (A) before and (B) after the electrodeposition of Pt nanoparticles.

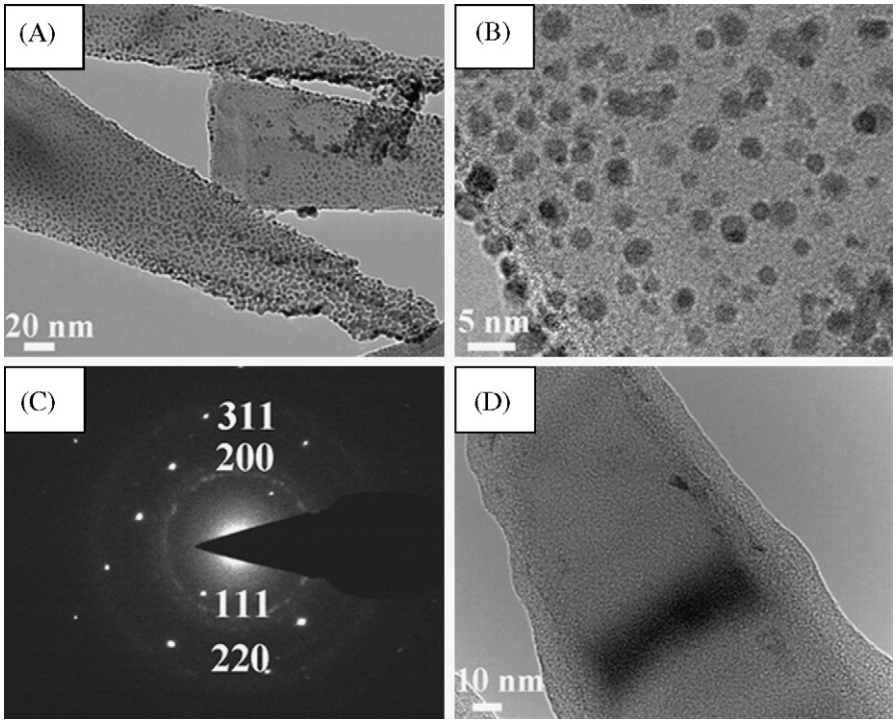

Fig. 3. (A) Bright-field TEM image of the α-C coated SNC with electrodeposited Pt nanoparticles, (B) high-resolution TEM image of the α-C coated SNC with Pt nanoparticles, (C) the SAD pattern, and (D) bright-field image of the α-C coated SNC without the Pt nanoparticle.

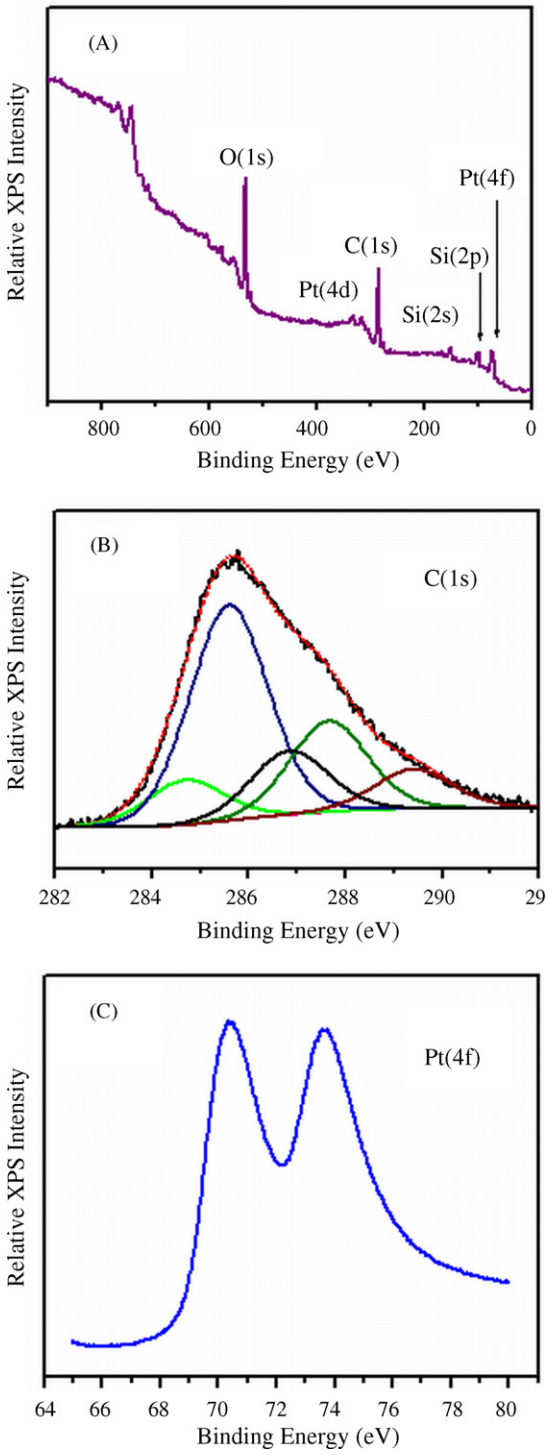

Fig. 4. (A) The wide scan XPS of the Pt nanoparticles deposited ACNC array, (B) the C(1s) XPS spectrum with curve-fitted peaks, and (C) the Pt(4f) XPS spectrum.

the (2 2 0) and (3 1 1) lattice planes could also be perceived but with a very weak intensity. The TEM analysis indicated that crystalline Pt nanoparticles were uniformly electrodeposited on the ACNCs.

Fig. 4(A) shows the XPS spectrum of the Pt loaded ACNC array. In addition to XPS signals due to Pt nanoparticles and the α-C overlayer, the XPS analysis also detected O(1s), Si(2p) and Si(2s) photoelectrons. The relatively strong O(1s) XPS signal suggested the presence of oxygen surface groups on the α-C layer. Curve fitting for the broad and asymmetric C(1s) XPS signal was performed assuming a Gaussian–Lorentzian curve with a half-width-at-full-

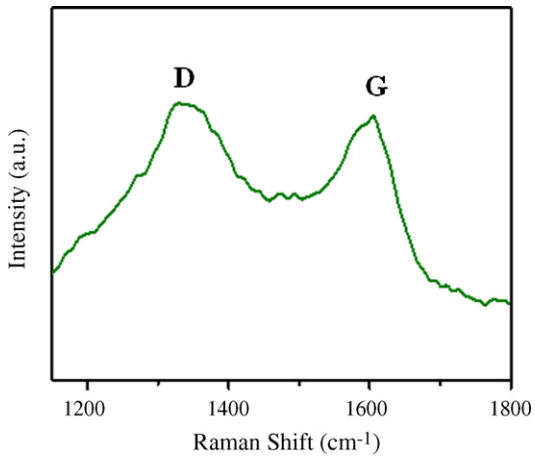

Fig. 5. Raman spectrum of the α-C coated SNCs without Pt nanoparticles.

maximum of 1.9 eV for all the synthesized peaks. The curve fitting result (Fig. 4(B)) revealed four chemical states with binding energies higher than that typically assigned to the C–C bonding and/or graphitic structure (~284.6 eV) [14]. The curve-fitted peaks at 285.6, 286.8, 287.6 and 289.4 eV can be ascribed to C–O–C, C–OH, C═O and –COOH (RCOO–) functional groups, respectively [15,16]. The Pt(4f) XPS spectrum shown in Fig. 4(C) exhibited a broad doublet peak with the Pt($4f_{7/2}$) peak maximum at 70.5 eV, which negatively shifted from that for bulk Pt by ~0.8 eV. As discussed later, we ascribe the negative binding energy shift of the Pt(4f) doublet peak to a combination effect of the Pt particle size and charge transfer between Pt nanoparticles and the ACNC support. Detection of the Si(2s) and Si(2p) XPS signals due to the Si nanocone substrate indicated that the thickness of the α-C layer was smaller than the probe depth of the Si(2s) and Si(2p) photoelectrons excited by the Mg Kα source, which was roughly less than 10 nm. The TEM analysis did show an α-C layer ~5–10 nm thick deposited on the SNC (Fig. 3(D)). Although thin, the α-C layer could greatly affect Pt electrodeposition and electrocatalytic characteristics of the Pt nanoparticles.

Fig. 5 shows the Raman spectrum in the range of 1150–1800 cm^{-1} of the ACNC array without the Pt catalyst. The two characteristic Raman peaks for disordered graphitic carbon materials in this range, the G and D peaks, were situated at ~1605 and ~1336 cm^{-1}, respectively. Peak features of both the Raman modes, such as peak position and intensity, greatly depend on the sp^2 bonding structure of CVD deposited carbon materials. The G peak is due to sp^2 bond stretching and the D peak is considered to be a ring breathing mode in a disordered graphitic structure [17]. The G peak is particularly useful to reveal nanocrystallinity of the graphitic structure [18]. When the size of the nanocrystalline graphite cluster is smaller than 2 nm, the G peak shifts to a position higher than 1600 cm^{-1} [17]. The peak position of the G mode at ~1605 cm^{-1} and the relative large D peak signal implied that a significant amount of nanosized graphitic structures were likely present in the α-C layer. Because of the disordered nanosized graphitic carbon structure, oxygen-containing species, such as those revealed by the XPS analysis, effectively adsorbed on edge defect sites of nanocrystalline graphite clusters in the α-C layer. The oxygen-containing adspecies acted as anchoring centers on the nanocone surface for the Pt precursor during Pt electrodeposition, thereby resulting in a better Pt dispersion [4]. As discussed latter, π-bondings on nanosized graphitic clusters of the α-C layer improved adhesion between Pt nanoparticles and the ACNC support, greatly alleviating agglomeration and loss of Pt nanoparticles during electrocatalytic reactions [9–11].

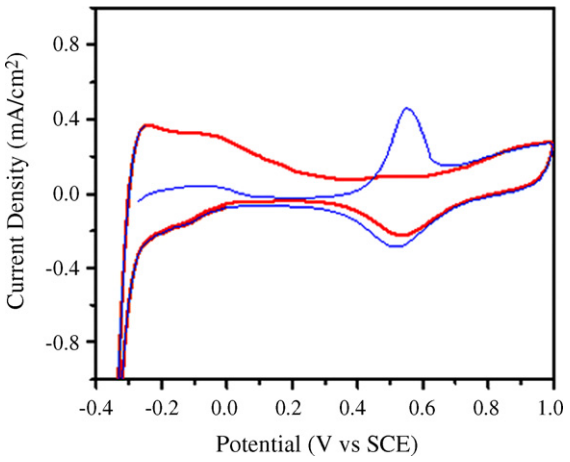

Fig. 6. CO-stripping cyclic voltammograms of the Pt/ACNC electrode in a CO saturated 1 M H_2SO_4 solution. The blue line is for the first potential scan and the red line for the second scan. The scan rate was 25 mV s^{-1}. (For interpretation of the references to color in this figure legend, the reader is referred to the web version of the article.)

3.2. Electrocatalytic activity

The electrochemical surface areas (ESAs) of the Pt/ACNC electrode were evaluated by CO-stripping cyclic voltammetry (CV), performed in a CO saturated 1 M H_2SO_4 aqueous solution using a Pt disk as the counter electrode and SCE as the reference electrode. For comparison, the ESA of a Pt film/Si electrode, prepared by electrodepositing a continuous Pt film on the flat Si substrate, was also measured. Fig. 6 shows a representative CO-stripping cyclic voltammogram for the Pt–ACNC electrode. A very high ESA of 327 m^2 g^{-1} was calculated for the Pt/ACNC electrode by integrating the electro-oxidation peak of adsorbed CO molecules, assuming an electro-oxidation charge of 420 μC cm^{-2} for a monolayer of CO adspecies on a smooth Pt surface [19]. The ESA of the Pt/ACNC electrode was about eight times higher than that of the Pt film/Si electrode and much higher than that of many previously reported electrodes of carbon materials [3,20,21]. The high ESA is ascribed to the large surface area of the nanocone array and the highly dispersed Pt nanoparticles. The geometric shape of ACNC support provided a surface area for Pt loading five times larger than that for the flat Si surface. The highly dispersed Pt nanoparticles also further increased the active surface area on the Pt/ACNC electrode.

Efficient removal of the CO adspecies from the Pt catalyst surface is crucial for minimizing the poisoning effect in DMFCs. The CO-stripping voltammograms of Fig. 6 also provide information about electro-oxidation of CO adspecies on the electrocatalyst. The onset potential of CO electro-oxidation on the Pt/ACNC and the Pt film/Si electrodes was about ~0.36 and ~0.51 V, respectively. The lower onset potential of the CO electro-oxidation and the higher ESA clearly demonstrates that the Pt/ACNC electrode could effectively improve the electroactivity of the Pt catalyst toward MOR. The improvement on electro-oxidation activity of CO adspecies on the Pt/ACNC electrode may be ascribed to the synergistic effect of the bi-functional mechanism and the Langmuir–Hinshelwood (L–H) mechanism. The LH mechanism is used to describe a bimolecular surface reaction, in which two adspecies diffuse on the surface, followed by collision and reaction with each other leading to formation of surface products [22]. The XPS analysis discussed above showed plenty of oxygen-containing adspecies on the α-C layer. The oxygen-containing surface groups surrounding the Pt catalyst particle can easily access and interact with CO adspecies in the peripheral region of Pt nanoparticles in terms of the bi-functional mechanism, and the nm-sized Pt catalyst allows fast migration of adspecies over the particle surface, thereby electro-oxidation of CO adspecies, in particular by –OH adspecies, can readily proceed via the L–H mechanism.

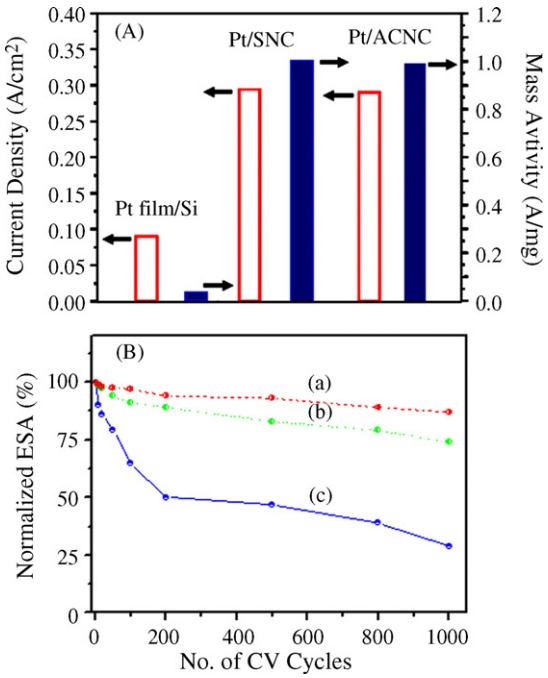

Fig. 7. (A) The current density (open bar) and the mass activity (solid bar) of the Pt/ACNC, Pt/SNC and Pt film/Si electrodes. (B) The loss of the Pt electrochemical surface area of (a) the Pt/ACNC, (b) Pt/SNC and (c) the Pt film/Si electrodes as a function of the number of CV cycles in argon saturated 1 M H_2SO_4 aqueous solution at room temperature (scan rate: 25 mV s^{-1}).

MOR activity of these two electrodes in the 1 M CH_3OH + 1 M H_2SO_4 aqueous solution at room temperature was studied by CV. Fig. 7(A) shows the current density and mass activity of the Pt film/Si and Pt/ACNC electrodes. Also shown in the figure is the electrocatalytic performance of the electrode with Pt nanoparticles electrodeposited on bare Si nanocones (Pt/SCN), which has been reported in our previous work [12]. The Pt/ACNC electrode had a mass activity and current density comparable to the Pt/SNC electrode, but much higher than the Pt film/Si electrode. The current density and mass activity of the Pt/ACNC electrode were ~4 and ~10 times that of the Pt film/Si electrode, respectively. Compared with many reported electrodes composed of carbon materials, such as carbon-coated anatase TiO_2 composites [3] and nanoporous materials synthesized by electrochemical lithiation [23], the Pt/ACNC electrode also exhibited better MOR performance in terms of catalyst mass activity and current density. The excellent MOR activity of the Pt/ACNC electrode can ascribe to the large ESA. In addition, the nm-sized Pt catalyst particles could enhance electro-oxidation of CO adspecies via the bi-functional and L–H mechanisms as discussed above, creating more active free sites for MOR and thus improving MOR efficiency.

Electrochemical stability of the Pt/ACNC, Pt/SCN and Pt film/Si electrodes for MOR was evaluated by CV within the potential range −0.4 to 1.2 V (vs. SCE) at a scan rate of 25 mV s^{-1} in an argon saturated 1 M H_2SO_4 aqueous solution for more than 1000 cycles. The ESA loss as a function of the number of CV cycles for the three electrodes is shown in Fig. 7(B). The Pt/ACNC electrode showed a very moderate reduction in the ESA during the repeating CV scans. The ESA of the Pt/ACNC electrode decreased by ~12% after 1000 CV cycles in the acid solution, while the Pt–SNC and Pt films/Si electrodes showed a decrease of ~22 and >50%, respectively, under the same electrochemical test condition. Fig. 8 shows the TEM images

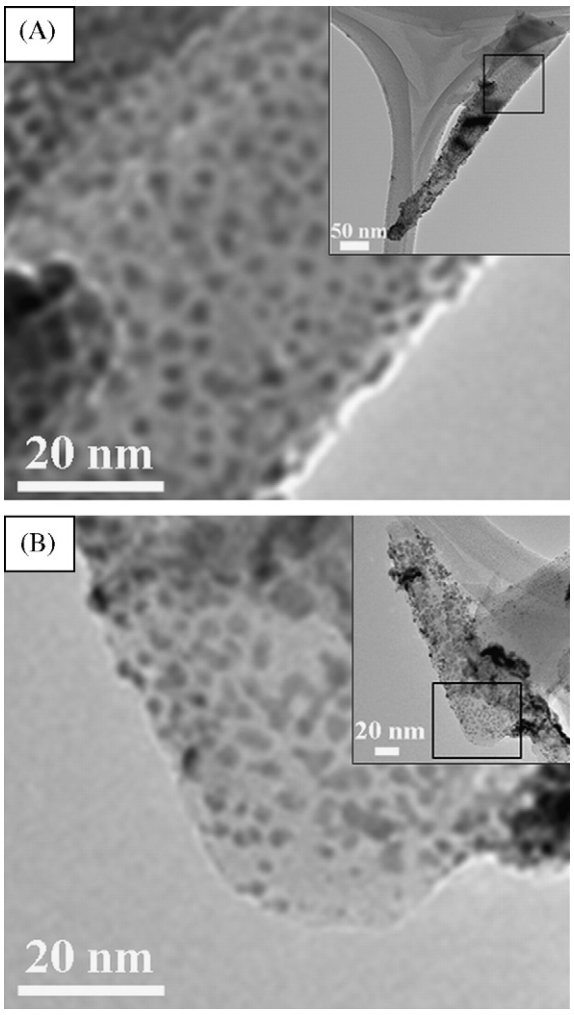

Fig. 8. The TEM images of the selected areas of an as-prepared Pt/ACNC nanocone (A) and a Pt/ACNC nanocone after the electrochemical stability test (B). The TEM images in the two insets have different magnification.

of an as-prepared Pt/ACNC nanocone and a Pt/ACNC nanocone subject to the electrochemical stability test. It should be noted that the nanocone TEM specimens were scratched off the Pt/ACNC array, which had millions of nanocones per square centimeter. Statistical diversity in morphology of ACNCs and Pt nanoparticles does not allow a decisive determination on the change in the Pt particle density and size before and after the electrochemical stability test by comparing two randomly selected nanocone TEM specimens. But a rough comparison can still provide useful information about the cause of the ESA loss. According to the TEM images, the Pt/ACNC seems to have a small decrease in the density of Pt nanoparticles with slight particle agglomeration. The loss of the ESA of the Pt catalyst might take place via two pathways: loss of the Pt catalyst from the support and agglomeration of Pt nanoparticles. The former may be due to detachment or dissolution of the Pt catalyst from the support during the electrochemical measurement. The later can decrease the surface to volume ratio of Pt particles and accordingly the particle density, thus resulting in a loss of the ESA. Because the size of isolated Pt nanoparticles does not show obvious change before and after the stability test according to Fig. 8, the small ESA loss of the Pt–ACNC electrode is very likely due to the mild agglomeration of Pt nanoparticles.

The much smaller ESA loss for the Pt/ACNC electrode compared with the Pt film/Si and Pt/SNC electrodes implied that Pt nanoparticles were relatively stable in the acidic electrolyte during the voltage scan. The nanocrystalline graphitic structure in the α-C layer as revealed by Raman scattering spectroscopy might play a crucial role in making the Pt/ACNC electrode much more stable toward MOR than the Pt film/Si electrode. In the broad Pt(4f) doublet XPS spectrum shown in Fig. 4(C), the Pt($4f_{7/2}$) peak reached a maximum at 70.5 eV, which was ~0.8 eV smaller than that of bulk Pt. The large red shift observed in the study might be a combination effect of the nm-sized Pt catalyst and the π-electron donation from the support to Pt nanoparticles. A red shift of 0.5 eV for the Pt(4f) doublet peaks have been reported for nm-sized (<3.0 nm) Pt colloids supported on highly oriented pyrolytic graphite [24]. The negative shift of the Pt(4f) doublet peak for Pt nanoparticles is generally ascribed to the reduced coordinated number of surface atoms in a nm-sized cluster [25,26]. Charge transfer between Pt nanoparticles and the support can also positively or negatively shift the Pt(4f) binding energies, depending on the chemical property of the support [27]. Because the red shift observed in the study is larger than reported values due to the nm-size effect, charge transfer from the α-C layer to the Pt catalyst is likely to occur, thus further decreasing the binding energy of the Pt(4f) electron. It has been widely reported that increasing the graphitization degree of carbon supports strengthens the metal-support interaction and enhances resistance against support oxidation and catalyst agglomeration [9–11,28]. Charge transfer between π-sites of the α-C layer and Pt nanoparticles can also alter the electronic structure of nm-sized Pt catalyst particles, thereby modifying electrocatalytic activities of the Pt catalyst toward MOR. In addition to electronically modifying Pt nanoparticles, the charge transfer interaction can also enhance the adhesion of electrodeposited Pt nanoparticles to the ACNC support, and thus prevent Pt nanoparticles from separating from the ACNC electrode.

The slow ORR rate on the cathode is always a concern for DMFC applicability. We have also studied electrocatalytic activity of the Pt/ACNC electrode toward ORR by the CV measurement. Fig. 9(A) shows typical ORR polarization curves of the Pt/ACNC, Pt/SCN and Pt film/Si electrodes, obtained in an O_2 saturated 1 M H_2SO_4 aqueous solution at room temperature. The ORR half-wave potentials for the Pt/ACNC, Pt/SCN and Pt film/Si electrodes were ~0.60, ~0.56 and ~0.52 V, respectively, and the ORR current densities were −7.4, −5.4 and −1.2 mA cm^{-2}, respectively. The current density of the Pt/ACNC electrode was six times higher than that of the Pt film/Si electrode, indicating that the Pt/ACNC electrode significantly enhanced the ORR rate. Compared with many previous reported electrodes, such as Pt catalysts with gold clusters [29], $Pt_3Ni(1\,1\,1)$ catalysts [30], supportless Pt and Pt–Pd nanotubes [31] and dealloyed Pt–Cu–Co nanoparticles [32], the Pt/ACNC electrode showed a higher peak current density as well. The great improvements on ORR electroactivity of the Pt catalyst on the ACNC support can be attributed to similar factors enhancing MOR electroactivity. The well-dispersed Pt nanoparticles on the ACNC support provided a large ESA leading to a faster reaction rate of ORR. The size of Pt nanoparticles affects the potential distribution within the double layer around the catalyst and also enhances the mass transport of electroactive species on the Pt catalyst [33].

The Pt/ACNC electrode also demonstrated excellent electrocatalytic stability for ORR. The electrocatalytic stability test was performed in an O_2 saturated 1 M H_2SO_4 aqueous solution at 25 °C. The CV measurement of more than 1000 cycles was conducted in the potential range between 0.2 and 0.8 V vs. SCE at a scan rate of 25 mV s^{-1}. Fig. 9(B) shows the ORR current density loss for the Pt/ACNC, Pt/SCN and Pt film/Si electrodes as a function of the number of CV cycles. The decrease in ORR activity of the Pt/ACNC, Pt/SCN and Pt film/Si electrodes after 1000 cycles was about ~16, ~18 and >60%, respectively. The better ORR activity stability of the Pt/ACNC electrode may also be due to the unique chemical properties of the

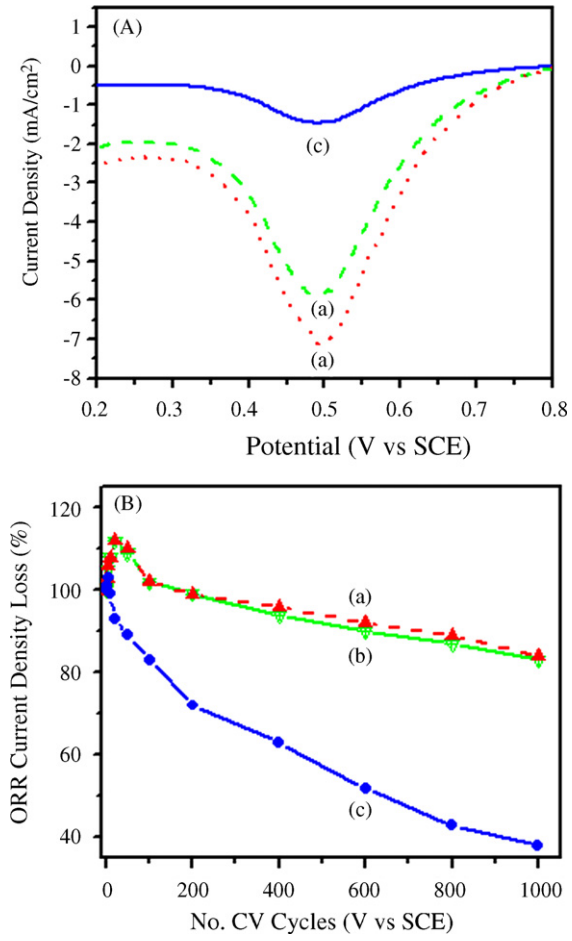

Fig. 9. (A) Cyclic voltammograms of ORR in O_2 saturated 1 M H_2SO_4 aqueous solution at 25 °C for (a) the Pt/ACNC (b) Pt/SNC and (c) Pt film/Si electrodes; and (B) ORR current density loss as a function of the number of cyclic voltammetry cycles in oxygen saturated 1 M H_2SO_4 at room temperature for (a) the Pt/ACNC, (b) Pt/SNC and (c) Pt film/Si electrodes (scan rate: 25 mV s^{-1}).

ACNC support, composed of nanocrystalline graphitic structures and full of oxygen-containing adspecies.

4. Conclusions

This work prepared highly order ACNC array as the support of pulse-electrodeposited Pt nanoparticles, and studied the electroactivity of the Pt–ACNC electrode toward MOR and ORR. Because nm-sized Pt catalyst particles were well dispersed on the ACNC support with a large surface area, the Pt/ACNC electrode had a large ESA. The electrocatalytic activity of the Pt/ANCN electrode was comparable to the electrode with Pt nanoparticles electrodeposited on bare Si nanocones (Pt/SNC) but with a better electrochemical stability. According to Raman scattering and XPS analyses, the ACNC array was composed of nanocrystalline graphitic structures, and full of oxygen-containing adspecies. The large negative Pt(4f) binding energy shift suggested the occurrence of charge transfer from π-sites of the graphitic structure in the α-C layer to the Pt nanoparticle. The charge transfer interaction cannot only alter the electronic structure of the Pt catalyst particle, thus modifying the electrocatalytic activity of the catalyst, but also enhance the adhesion of the nanoparticle to the ACNC support. The presence of oxygen-containing adspecies on the ACNC support and the nanometer scale of Pt catalyst particles are proposed to be the main causes enhancing the CO electro-oxidation via the bi-functional mechanism and L–H mechanism, thereby improving the resistance of the Pt/ACNC electrode against CO poisoning and thus improving the electrocatalytic activity toward MOR.

Acknowledgments

This work was supported by the National Science Council of R.O.C., under Contract No. NSC93-2120-M-009-007. We thank the National Nano Device Laboratories (NDL) for the technical support.

References

[1] S.H. Joo, S.J. Choi, I. Oh, J. Kwak, Z. Liu, O. Terasaki, R. Ryoo, Nature 412 (2001) 169.
[2] T. Hyeon, S. Han, Y.-E. Sung, K.W. Park, Y.W. Kim, Angew. Chem. Int. Ed. 42 (2003) 4352.
[3] S. Shanmugam, A. Gedanken, Small 3 (2007) 1189.
[4] F. Rodriguez-Reinoso, Carbon 36 (1998) 159.
[5] J. Zeng, F. Su, J.Y. Lee, W. Zhou, X.S. Zhao, Carbon 44 (2006) 1713.
[6] W. Xu, X. Zhou, C. Liu, W. Xing, T. Lu, Electrochem. Commun. 9 (2007) 1002.
[7] W. Chen, Q. Xin, G. Sun, Q. Wang, Q. Mao, H. Su, J. Power Sources 180 (2008) 199.
[8] J.D. Carey, S.R.P. Silva, Phys. Rev. B 70 (2004) 235417.
[9] F. Coloma, A. Sepulveda-Escribano, J.L.G. Fierro, Langmuir 10 (1994) 750.
[10] Y.Y. Shao, G.P. Yin, Y.Z. Gao, J. Power Sources 171 (2007) 558.
[11] X.W. Yu, S.Y. Ye, J. Power Sources 172 (2007) 145.
[12] J.N. Tiwari, T.-M. Chen, F.M. Pan, K.-L. Lin, J. Power Sources 182 (2008) 510.
[13] T.M. Chen, F.M. Pan, J.Y. Hung, L. Chang, S.C. Wu, C.F. Chen, J. Electrochem. Soc. 154 (2007) D215.
[14] T.L. Barr, M. Yin, J. Vac. Sci. Technol. A 10 (1992) 2788.
[15] S. Biniak, G. Szymanski, J. Siedlewski, A. Swiatkowski, Carbon 35 (1997) 1799.
[16] E.A. Hoffmanna, T. Kortvelyesia, E. Wiluszb, L.S. Korugic-Karaszc, F.E. Karaszc, Z.A. Feketea, J. Mol. Struct. Theochem 725 (2005) 5.
[17] A.C. Ferrari, J. Robertson, Phys. Rev. B 61 (2000) 14095.
[18] M.A. Tamor, W.C. Vassell, J. Appl. Phys. 76 (1994) 3823.
[19] J.W. Guo, T.S. Zhao, J. Prabhuram, R. Chen, C.W. Wong, Electrochim. Acta 51 (2005) 754.
[20] A. Guha, T.A. Zawodzinski, D.A. Schiraldi, J. Power Sources 172 (2007) 530.
[21] A. Pozio, M. De Francesco, A. Cemmi, F. Cardellini, L. Giorgi, J. Power Sources 105 (2002) 13.
[22] R.J. Baxter, P. Hu, J. Chem. Phys. 116 (2002) 4379.
[23] Y.S. Hu, Y.-G. Guo, W. Sigle, S. Hore, P. Balaya, J. Maier, Nat. Mater. 5 (2006) 713.
[24] Sh.K. Shaikhutdinov, M. Schildenberger, M. Noeske, G. Mestl, React. Kinet. Catal. Lett. 67 (1999) 129.
[25] X. Wang, J.C. Yu, H.Y. Yip, L. Wu, P.K. Wong, S.Y. Lai, Chem. Eur. J 11 (2005) 2997.
[26] J. Radnik, C. Mohr, P. Claus, Phys. Chem. Chem. Phys. 5 (2003) 172.
[27] J.R. Croy, S. Mostafa, J. Liu, Y. Sohn, H. Heinrich, B.R. Cuenya, Catal. Lett. 119 (2007) 209.
[28] Y. Li, F.P. Hu, X. Wang, P.K. Shen, Electrochem. Commun. 10 (2008) 1101.
[29] J. Zhang, K. Sasaki, E. Sutter, R.R. Adzic, Science 315 (2007) 220.
[30] V.R. Stamenkovic, B. Fowler, B.S. Mun, G. Wang, P.N. Ross, C.A. Lucas, N.M. Marković, Science 315 (2007) 493.
[31] Z. Chen, M. Waje, W. Li, Y. Yan, Angew. Chem. Int. Ed. 46 (2007) 4060.
[32] R. Srivastava, P. Mani, N. Hahn, P. Strasser, Angew. Chem. Int. Ed. 46 (2007) 8988.
[33] S. Chen, A. Kucernak, J. Phys. Chem. B 108 (2004) 3262.